HAL open science

Thermodynamics of Extra-Toughness and Hidden-Length in Polymeric Materials with Sacrificial Bonds

Romain Jorge Do Marco, Stefano Giordano

▶ **To cite this version:**

Romain Jorge Do Marco, Stefano Giordano. Thermodynamics of Extra-Toughness and Hidden-Length in Polymeric Materials with Sacrificial Bonds. Applied Mechanics, 2022, 3 (3), pp.935-955. 10.3390/applmech3030053 . hal-03776029

HAL Id: hal-03776029

https://hal.science/hal-03776029v1

Submitted on 13 Sep 2022

HAL is a multi-disciplinary open access archive for the deposit and dissemination of scientific research documents, whether they are published or not. The documents may come from teaching and research institutions in France or abroad, or from public or private research centers.

L'archive ouverte pluridisciplinaire **HAL**, est destinée au dépôt et à la diffusion de documents scientifiques de niveau recherche, publiés ou non, émanant des établissements d'enseignement et de recherche français ou étrangers, des laboratoires publics ou privés.

Distributed under a Creative Commons Attribution 4.0 International License

applied mechanics

MDPI

Article

Thermodynamics of Extra-Toughness and Hidden-Length in Polymeric Materials with Sacrificial Bonds

Romain Jorge Do Marco and Stefano Giordano *

Univ. Lille, CNRS, Centrale Lille, Univ. Polytechnique Hauts-de-France, UMR 8520—IEMN—Institut d'Electronique de Microélectronique et de Nanotechnologie, F-59000 Lille, France; romain.jorge-do-marco@centrale.centralelille.fr

* Correspondence: stefano.giordano@univ-lille.fr

Abstract: Sacrificial bonds have been observed in several biological materials and structures and can increase their toughness, i.e., their resistance to fracture. They provide a reversible mechanism for dissipating mechanical energy before the possible system rupture. From a structural point of view, sacrificial bonds consist of short polymer chains that short-circuit parts of a main macromolecular chain (generating hidden lengths) and absorb energy by breaking them instead of the main chain. The toughness increase due to the presence of sacrificial bonds is typically named extra-toughness. Here, we developed a statistical mechanics and thermodynamics-based theory able to estimate the force–extension relation for chains with sacrificial bonds and to calculate the corresponding extra-toughness. The model is useful to better understand the sacrificial bond effects in biomaterials but also to apply the biomimetic paradigm and foster the development of high-performance artificial polymeric materials.

Keywords: sacrificial bonds; statistical mechanics; force–extension relation; spin variables

check for updates

Citation: Jorge Do Marco, R.; Giordano, S. Thermodynamics of Extra-Toughness and Hidden-Length in Polymeric Materials with Sacrificial Bonds. *Appl. Mech.* **2022**, *3*, 935–955. https://doi.org/10.3390/applmech3030053

Received: 18 June 2022
Accepted: 25 July 2022
Published: 31 July 2022

Publisher's Note: MDPI stays neutral with regard to jurisdictional claims in published maps and institutional affiliations.

Copyright: © 2022 by the authors. Licensee MDPI, Basel, Switzerland. This article is an open access article distributed under the terms and conditions of the Creative Commons Attribution (CC BY) license (https://creativecommons.org/licenses/by/4.0/).

1. Introduction

Several materials and structures of biological origin have much higher toughness than most artificial materials. The explanation for this exceptional property lies in a particular microstructure observed at the molecular level and recently probed by means of force spectroscopy techniques. Many studies have indeed revealed that the toughening mechanism is based on sacrificial bonds and hidden lengths [1–3]. Sacrificial bonds are defined as polymer chains designed to break when the system is subjected to mechanical action before the main macromolecular chain [4,5]. In this sense, they protect the main system from breakdown by sacrificing themselves in its place. Considering the main chain, sacrificial bonds are rather short chains that short-circuit much longer sections of the main chain and, therefore, generate the so-called hidden lengths in the system (see Figure 1). These sacrificial bonds are typically weaker from the mechanical point of view with respect to the covalent bonds of the main macromolecule. So, when the force is applied to the system, it can break by adsorbing a large amount of energy and releasing the hidden lengths. Then, when the force is removed, they are typically self-repaired because of the reversibility of the process. The characteristic force–extension relation of a chain with sacrificial bonds is characterized by a series of peak forces (corresponding to the breaking of a sacrificial bond), which is named the sawtooth pattern [6,7].

Concerning biological materials, a complex microstructure (including calcium-mediated sacrificial bonds) has been observed in the organic matrix of bones [8,9]. Scientists proved that the time necessary for these sacrificial bonds to reconstitute after the stress-removing corresponds to the time necessary to recover the original bone toughness, as measured by atomic force microscope indentation testing [10]. Moreover, it has been observed that the recluse spider (Loxosceles genus) spins its silk ribbons into sacrificial micro-loops, which are very efficient to improve the toughness [11]. Interestingly, sacrificial bonds

provide the strong adhesive properties of gastroliths (or stomach stones) as well [12]. Other hierarchical microstructural strategies can be observed in different natural materials, such as nacre shells, muscle sarcomeres, and collagen fibrils, which are remarkable examples of high-performance systems [13–15].

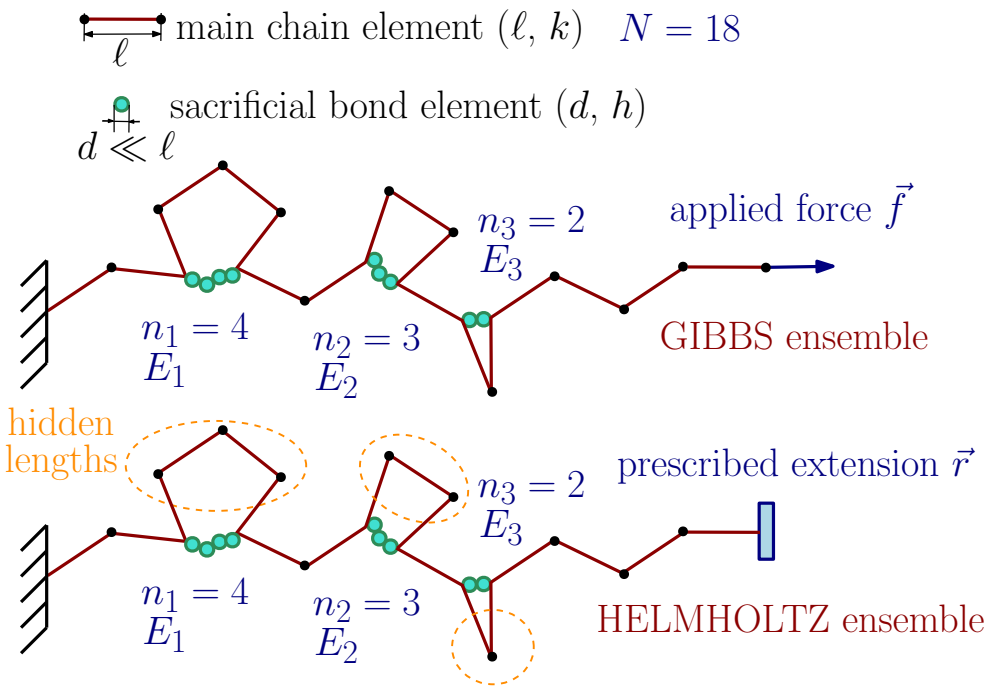

Figure 1. Simplified sketch of a polymer chain or macromolecule with sacrificial bonds. The main chain is composed of N. elements with the equilibrium length ℓ and elastic constant k. Each sacrificial bond is composed of n_j elements with equilibrium length $d \ll \ell$ and elastic constant h, and is characterized by fracture energy E_j (where $j = 1, ..., s$, with s being the number of sacrificial bonds). The chain is studied within the Gibbs ensemble (with an applied force) and within the Helmholtz ensemble (with prescribed extension). The main chain elements short-circuited by the sacrificial bonds correspond to the hidden lengths of the system.

The study of the properties of systems with toughening sacrificial bonds is not only important for the deep understanding of the biological structures but also for developing bio-inspired artificial polymeric materials with exceptional mechanical properties [1,16]. Indeed, mimicking the biological structures by following the biomimetic approach is one of the main avenues for developing new high-performance synthetic polymeric materials based on hierarchical structures and various types of organic and inorganic molecules [17–21]. For example, sacrificial metal–ligand bonds can be added into elastomers [22], elastomer/graphene composites [23], glycogen-based hydrogels [24], or a composite double network ionic hydrogel (CDN-gel) [25]. Moreover, bioinspired tunable sacrificial bonds are successfully introduced into the tetra-poly(ethylene glycol) (PEG)-based polyurethane (PU) (TP) hydrogel network [26]. It has been proven that an acrylate polymer, typically showing a brittle solid state fracture, can become defect-tolerant by adding energy dissipating supramolecular interactions [27]. Moreover, artificial muscles have been developed through sacrificial coordination networks [28]. To toughen the epoxy resin, a renewable system of sacrificial bonds has been prepared with a modified tung oil [29]. These are just some examples, and many others can be found in the literature. The beneficial effects of sacrificial bonds in several materials have been observed by means of chemiluminescent cross-linking molecules, which emit light when they break. They have been used to directly follow (in real-time) the propagation of a crack in a given structure [30,31].

Although some mathematical models and numerical analyses on systems having sacrificial bonds can be found in the literature [3–7,17], a complete theory based on statistical mechanics and thermodynamics has not been formulated for the moment. The purpose of this paper is to fill this gap by proposing a theory based on equilibrium statistical mechanics and on the so-called spin variables method. The need to use statistical mechanics and thermodynamics to approach this problem comes from the fact that, given the size and energies involved, thermal fluctuations are crucial in determining the behavior of the system. In other words, entropic forces are of the same order of magnitude as enthalpic forces and cannot be neglected. The theoretical modeling of the thermomechanical response of macromolecules (polymers, proteins, nucleic acids, and so on) [32–34] has been strongly stimulated by the advent of force spectroscopy methods (AFM, optical tweezers, magnetic tweezers, MEMS, and NEMS) which offer the possibility of directly probing the force–extension response of single chains [35–39]. Classical theories include the freely-jointed chain (FJC) model [40–42] (describing, e.g., single-stranded DNA and RNA) or the worm-like chain (WLC) model [43–46] (well representing the double-stranded DNA behavior). Further, these models have been generalized in order to take into account the conformational transitions in proteins and other two-state (or multi-state) macromolecules [47–55]. Indeed, many chains of biological origin are composed of domains that exhibit the possible switching between two or more states or conformations, depending on the mechanical action applied and on the system temperature [56–58]. Moreover, it is interesting to note that other artificial mechanical systems show similar transitions, induced by a multi-basin energy landscape [59–62]. A particularly efficient method to model the force–extension relation of two-state systems is the so-called spin variables approach. In order to distinguish the two states of a chain domain (typically named folded and unfolded) a discrete variable—assuming only two values—is introduced (it behaves as a bit or a spin). Then, the statistical mechanics of the system is developed by considering the classical continuous variables (position of domains) and the additional spin variables (state of domains), allowing for the calculation of the pertinent partition functions and the elaboration of the macroscopic thermodynamics. This approach was first introduced to model the behaviors of muscle fibers [63,64], and is still used to study the muscle system [65–67]. Today, it has been generalized to study different biophysical phenomena, including macromolecular elasticity [68–75] and adhesion mechanisms [76,77].

In this work, the spin variables are used to distinguish the intact state and the broken state of the sacrificial bonds included in the system. The chain is represented by a generalization of the classical freely-jointed chain (FJC), with an additional distribution of sacrificial bonds. This approach is able to automatically show the transitions between the states as functions of the applied load and thermal conditions. Interestingly, this method allowed us to investigate the force–extension relation in both the Helmholtz ensemble (with the prescribed extension of the main chain) and the Gibbs ensemble (with an applied force to the main chain), see Figure 1 [68]. The partition functions for both cases can be calculated in closed form and the corresponding thermodynamics (macroscopic behavior) can be directly investigated. In particular, the multi-plateau behavior of the force–extension response was obtained for the Gibbs ensemble and the sawtooth pattern with peaks of force was observed for the Helmholtz ensemble. As expected, the two statistical ensembles show different force–extension responses for a finite number N of elements of the chain [68]. We studied these curves for an arbitrary number of sacrificial bonds within the main chain and for an arbitrary distribution of sacrificial bond lengths and fracture energies. Indeed, each sacrificial bond is characterized by its length and fracture energy, representing the amount of energy necessary to break the bond itself. The knowledge of the force–extension curve is important to evaluate the extra-toughness, defined as the increase in the area under the curve by moving from the case without sacrificial bonds to the case with sacrificial bonds (see Figure 2).

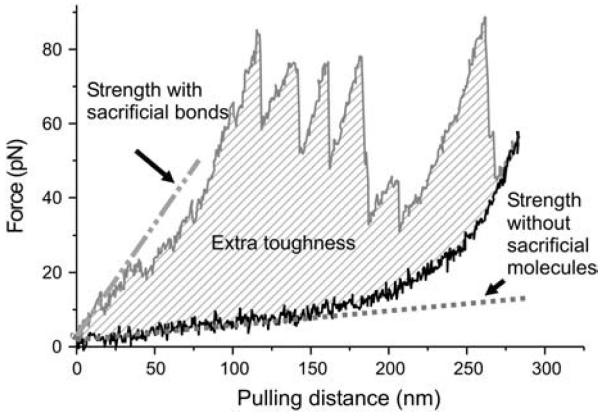

Figure 2. Sacrificial bonds increase the toughness of a material. The extra-energy (or extra-toughness) adsorbed and dissipated through the sacrificial molecules (shaded area in the curve) is a measure of the increase in toughness of the material. Moreover, the initial slope of the pulling curve can be modified by the sacrificial bonds (dash–dotted line with the sacrificial bonds and dotted line without the sacrificial bonds). We can also see the sawtooth pattern of the force–extension response. Reprinted with permission from Reference [3]. Copyright 2006 Elsevier.

It basically represents the energy that the system is able to absorb and dissipate without breaking the main structure of the chain. Therefore, this parameter measures the enhancement in the resistance to the fracture. Interestingly, the model can be used to optimize the chain microstructure in order to have the maximal or the desired toughness. Eventually, it can be used to investigate the sacrificial bond features in biomaterials and to analyze and synthesize new artificial polymeric materials.

2. Force–Extension Response of a Chain with Sacrificial Bonds

In order to have a complete description of the sacrificial bond mechanics and thermodynamics, we will develop an analytic formalism for both the Gibbs ensemble (with applied force) and the Helmholtz ensemble (with prescribed extension), as discussed in the Introduction [68]. The system under consideration is a chain composed of N identical elements or segments described by the so-called extensible freely-jointed chain (FJC) interaction scheme. These elements, in the simple chain without sacrificial bonds, will be described by the elastic stiffness k and the equilibrium length ℓ (see Figure 1). The chain is supposed to fluctuate in the three-dimensional space and is placed in a thermal bath at temperature T. Of course, several chains of biological origin exhibit a given persistence length, which could be taken into account only through the worm-like chain (WLC) model. However, we neglect here this issue in order to simplify the analysis and better focus on the sacrificial bond features.

We will now introduce the structure and geometry of the sacrificial bonds. Let s be the number of sacrificial bonds considered within this system. Each sacrificial bond connects two points of the original chain that include n_j elements, with $j = 1, ..., s$. Moreover, each sacrificial bond is composed of n_j elastic segments with a defined stiffness h and a defined equilibrium length $d \ll \ell$ (see Figure 1). This means that the part of the original chain (n_j elements characterized by k and ℓ) short-circuited by a sacrificial bond (n_j elements characterized by h and d) practically does not participate in the elasticity of the whole chain. The sequence of numbers n_j, with $j = 1, ..., s$, represents the size of the bonds, which can be heterogeneous in the most general case. Only when $n_j = n$ for all $j = 1, ..., s$ the system of sacrificial bonds is homogeneous. We consider the simplifying assumption that sacrificial bonds are never overlapping; that is, they never cross. This means that we must assume that $\sum_{j=1}^{s} n_j < N$. A chain without sacrificial bonds shows an equilibrium contour length equal to $N\ell$. However, a chain with all sacrificial bonds intact shows an equilibrium contour length equal to $(N - \sum_{j=1}^{s} n_j)\ell + \sum_{j=1}^{s} n_j d$. The difference between these two quantities, equal to $\sum_{j=1}^{s} n_j(\ell - d)$ is called the hidden length since it is a length

that cannot be measured when all sacrificial bonds are intact, i.e., at the beginning of any traction experiment (see Figure 1). Moreover, it is necessary to define a sequence E_j, with $j = 1, ..., s$, representing the rupture or breaking energies of the sacrificial bonds. It means that the value E_j represents the energy necessary to break the j-th sacrificial bond. It is important to underline that the system is able to adsorb the energy $\sum_{j=1}^{s} E_j$ before the breaking of the main chain. In this sense, sacrificial bonds act as mechanical fuses. During the traction of the chain, one or more of the sacrificial bonds may break; therefore, it is necessary to distinguish the broken bonds from the intact ones. Let y_j be a sequence of binary or spin variables defined, such that $y_j = 0$ when the j-th bond is broken and $y_j = 1$ when it is intact. We discuss below the separate analysis of the Gibbs and the Helmholtz boundary conditions.

2.1. Isotensional Gibbs Condition

We start by writing the total potential energy of the system under the Gibbs condition. Let K_b be Boltzmann's constant, T the temperature of the system, and $\vec{r}_i$, $i = 0, ..., N$ the sequence of positions delimiting the elements of the chain. We consider that the first element of the chain is tethered at the origin of the reference frame; thus, we assume $\vec{r}_0 = 0$. In addition, let $\vec{f}$ be the force applied on the last element of the chain. Under these assumptions, it is possible to write the total energy of the system as

$$\begin{aligned} E(\{\vec{r}_i\}, \{y_i\}) \quad = \quad & \sum_{i=1}^{N-\sum_{j=1}^{s} n_j y_j} \frac{1}{2} k(\|\vec{r}_i - \vec{r}_{i-1}\| - \ell)^2 \\ & + \sum_{i=N+1-\sum_{j=1}^{s} n_j y_j}^{N} \frac{1}{2} h(\|\vec{r}_i - \vec{r}_{i-1}\| - d)^2 \\ & + \sum_{j=1}^{s} E_j(1 - y_j) - \vec{f} \cdot \vec{r}_N. \end{aligned} \tag{1}$$

Here, depending on the values of the spin variables $y_i \in \{0, 1\}$, we can take into account all the possible configurations of the chain, represented by all combinations of broken or intact sacrificial bonds. We did not consider the kinetic energy entering the Hamiltonian of the system since it merely produces a non- influential multiplicative constant in the partition function. Indeed, due to the use of orthogonal coordinates, the kinetic energy depends only on the linear momentum variables and the potential energy only on the geometrical variables. Therefore, the two contributions are fully uncoupled and the integral over the momentum variables simply generates a multiplicative constant. Moreover, it is important to point out that in Equation (1) we considered all sacrificial bonds at the end of the chain but this does not affect the generality (since in the considered extensible freely-jointed chain model the order of the elements does not affect the overall elastic and thermodynamic responses) [69]. This is because there are no interactions between the adjacent elements in the chain.

The expression for the total energy of the system allows us to introduce the partition function for the Gibbs ensemble of the statistical mechanics [32,41]

$$Z_G(\vec{f}) = \sum_{\vec{y} \in \{0,1\}^s} \int_{\mathbb{R}^{3N}} e^{-\frac{E(\{\vec{r}_i\}, \{y_i\})}{K_b T}} d\vec{r}_1 ... d\vec{r}_N, \tag{2}$$

where $\vec{y} = (y_1, ..., y_s)$ is the vector of the spin variables. The integral can be elaborated by means of the change of variables $\vec{\xi}_1 = \vec{r}_1 - \vec{r}_0$, $\vec{\xi}_2 = \vec{r}_2 - \vec{r}_1$,..., $\vec{\xi}_N = \vec{r}_N - \vec{r}_{N-1}$, leading to $\sum_{k=1}^{N} \vec{\xi}_k = \vec{r}_N - \vec{r}_0$ and $d\vec{r}_1 ... d\vec{r}_N = d\vec{\xi}_1 ... d\vec{\xi}_N$. By fixing $\vec{r}_0$ at the origin of axes, we obtain

$$Z_G(\vec{f}) = \sum_{\vec{y} \in \{0,1\}^s} \int_{\mathbb{R}^{3N}} e^{-\frac{E(\{\vec{\xi}_i\}, \{y_i\})}{K_b T}} d\vec{\xi}_1 ... d\vec{\xi}_N, \tag{3}$$

where

$$\begin{aligned} E\left(\left\{\vec{\xi}_i\right\},\{y_i\}\right) &= \sum_{i=1}^{N-\sum_{j=1}^{s} n_j y_j} \frac{1}{2}k\left(\|\vec{\xi}_i\|-\ell\right)^2 \\ &+ \sum_{i=N+1-\sum_{j=1}^{s} n_j y_j}^{N} \frac{1}{2}h\left(\|\vec{\xi}_i\|-d\right)^2 \\ &+ \sum_{j=1}^{s} E_j(1-y_j) - \vec{f}\cdot\sum_{i=1}^{N}\vec{\xi}_i. \end{aligned} \tag{4}$$

This expression can be rewritten as follows, in order to simplify the following calculations

$$\begin{aligned} E\left(\left\{\vec{\xi}_i\right\},\{y_i\}\right) &= \sum_{j=1}^{s} E_j(1-y_j) \\ &+ \sum_{i=1}^{N-\sum_{j=1}^{s} n_j y_j} \left(\frac{1}{2}k\left(\|\vec{\xi}_i\|-\ell\right)^2 - \vec{f}\cdot\vec{\xi}_i\right) \\ &+ \sum_{i=N+1-\sum_{j=1}^{s} n_j y_j}^{N} \left(\frac{1}{2}h\left(\|\vec{\xi}_i\|-d\right)^2 - \vec{f}\cdot\vec{\xi}_i\right). \end{aligned} \tag{5}$$

Then, it is possible to substitute Equation (5) into Equation (3) to obtain the expression

$$\begin{aligned} Z_G(\vec{f}) &= \sum_{\vec{y}\in\{0,1\}^s} e^{-\sum_{i=1}^{s}\frac{E_i}{K_bT}(1-y_i)} \\ &\times [\mathcal{F}(k,l)]^{N-\sum_{j=1}^{s} n_j y_j}[\mathcal{F}(h,d)]^{\sum_{j=1}^{s} n_j y_j}, \end{aligned} \tag{6}$$

where we introduce the function $\mathcal{F}(x,y)$, defined below

$$\mathcal{F}(x,y) = \int_{\mathbb{R}^3} e^{-\frac{x}{2K_bT}(\|\vec{\xi}\|-y)+\vec{f}\cdot\vec{\xi}} d\vec{\xi}. \tag{7}$$

To evaluate this integral, we assume (without limiting the generality) that the force is aligned to the third axis of the reference frame, $\vec{f} = (0,0,f)$. Indeed, the chain behavior is isotropic in the three-dimensional space. In addition, we change the variables according to $\vec{\xi} = (\xi\cos\varphi\sin\vartheta, \xi\sin\varphi\sin\vartheta, \xi\cos\vartheta)$. Since $d\vec{\xi} = \xi^2\sin\vartheta d\xi d\varphi d\vartheta$, $\|\vec{\xi}\| = \xi$ and $\vec{f}\cdot\vec{\xi} = f\xi\cos\vartheta$, we obtain the following simpler form for the function $\mathcal{F}(x,y)$

$$\mathcal{F}(x,y) = 4\pi\int_0^\infty e^{-\frac{x}{2K_bT}(\xi-y)^2}\frac{\sinh\left(\frac{f\xi}{K_bT}\right)}{\frac{f\xi}{K_bT}}\xi^2 d\xi. \tag{8}$$

From now on, we assume that the elastic constants k and h are large enough to justify the use of the freely-jointed chain scheme (without extensibility). To this aim, we can use the Dirac delta function property $\sqrt{\frac{\alpha}{\pi}}e^{-\alpha(x-x_0)^2} \underset{\alpha\to\infty}{\to} \delta(x-x_0)$, eventually yielding

$$\mathcal{F}(x,y) = 2(2\pi K_bT)^{\frac{3}{2}}\frac{y}{f\sqrt{x}}\sinh\frac{fy}{K_bT}. \tag{9}$$

To lighten the expression of the Gibbs partition function, we introduce the following notations

$$A(f) = \frac{l}{f\sqrt{k}}\sinh\frac{f\ell}{K_bT}, \tag{10}$$

$$B(f) = \frac{d}{f\sqrt{h}} \sinh \frac{fd}{K_b T}, \tag{11}$$

$$C_j = e^{-\frac{E_j}{K_b T}}, \tag{12}$$

and we obtain

$$Z_G(f) = A^N \sum_{\vec{y}\in\{0,1\}^s} \left(\prod_{i=1}^{s} C_j^{1-y_j} \right) A^{-\sum_{j=1}^{s} n_j y_j} B^{\sum_{j=1}^{s} n_j y_j} \tag{13}$$

$$= \left(\prod_{i=1}^{s} C_j \right) A^N \sum_{\vec{y}\in\{0,1\}^s} \left(\prod_{i=1}^{s} C_j^{-y_j} \right) \left(\frac{B}{A} \right)^{\sum_{j=1}^{s} n_j y_j}. \tag{14}$$

Please note that, in the definitions of $A(f)$ and $B(f)$, we left out the multiplicative constant $2(2\pi K_b T)^{\frac{3}{2}}$, which is irrelevant in the subsequent calculations. To conclude, it is necessary to note that, for each binary parameter y_i, there are two possible values $y_i = 0$ or $y_i = 1$. Therefore, we obtain the final result in the form

$$Z_G(f) = \left(\prod_{i=1}^{s} C_j \right) A^N \prod_{j=1}^{s} \left(1 + C_j^{-1} \left(\frac{B}{A} \right)^{n_j} \right). \tag{15}$$

This is the main achievement concerning the behavior of the ideal chain with sacrificial bonds under the isotensional Gibbs condition.

In order to study the Helmholtz ensemble, we have to further develop the second product in Equation (15). Let ϕ_i be a sequence of real numbers; we attempt to calculate the following product

$$P = \prod_{i=1}^{s} (1 + \phi_i). \tag{16}$$

By developing the expression, we directly have

$$P = 1 + \sum_j \phi_j + \sum_{i\neq j} \phi_i \phi_j + ... + \prod_{i=1}^{s} \phi_i, \tag{17}$$

where the sum contains 2^s terms. To simplify this expression, it is possible to use the bits of a number t between 0 and $2^s - 1$, written in base 2. If $\vec{t} = (t_1, ..., t_s)$ is the vector of the binary representation of the number t, then we can write

$$\prod_{i=1}^{s} (1 + \phi_i) = \sum_{t=0}^{2^s-1} \left(\prod_{j=1}^{s} \phi_j^{t_j} \right). \tag{18}$$

A trivial generalization of this result follows

$$\prod_{i=1}^{s} (a + \phi_i b) = \sum_{t=0}^{2^s-1} \left(\prod_{j=1}^{s} \phi_j^{t_j} \right) a^{s-\sum_{i=1}^{s} t_i} b^{\sum_{i=1}^{s} t_i}. \tag{19}$$

The application of this approach to Equation (15) immediately leads to

$$Z_G(f) = \sum_{t=0}^{2^s-1} \left(\prod_{i=1}^{s} C_i^{1-t_i} \right) A(f)^{N-\vec{n}\cdot\vec{t}} B(f)^{\vec{n}\cdot\vec{t}}, \tag{20}$$

where $\vec{n} = (n_1, ..., n_s)$ is the vector of the sacrificial bond lengths. The force–extension response for the chain with sacrificial bonds within the Gibbs ensemble can be found through the standard relation [32,41]

$$\langle r \rangle = k_B T \frac{\partial \log Z_G(f)}{\partial f}, \tag{21}$$

which will be used in the following developments to discuss the behavior of the system with an applied force. In this case, the average value of the extension is written as a function of the deterministic applied force.

2.2. Isometric Helmholtz Condition

The Helmholtz ensemble is characterized by the prescribed extension r of the chain, which assumes a deterministic character. Consequently, we will determine the average value $\langle f \rangle$ of the force, which is a random variable subjected to statistical fluctuations. We determine the Helmholtz partition function on the base of the previously evaluated Gibbs partition function. Indeed, it is possible to write the relationship [32,41]

$$Z_H(r) = \int_{-\infty}^{+\infty} Z_G(i\eta) \frac{\eta}{r} \sin\left(\frac{\eta r}{K_b T}\right) d\eta, \tag{22}$$

where $Z_G(i\eta)$ represents the analytic continuation of $Z_G(f)$ over the imaginary axis. Please note that the Fourier or Laplace relation between Z_H and Z_G is always true whereas the Legendre transform between the Helmholtz and Gibbs free energies is correct only when $N \to \infty$ (thermodynamic limit) [32,41]. By substituting the Gibbs partition function in Equation (22), we obtain

$$\begin{aligned} Z_H(r) &= \sum_{t=0}^{2^s-1} \left(\prod_{i=1}^{s} C_i^{1-t_i} \right) \int_{-\infty}^{+\infty} A(i\eta)^{N-\vec{n}\cdot\vec{t}} B(i\eta)^{\vec{n}\cdot\vec{t}} \sin\left(\frac{\eta r}{K_b T}\right) \frac{\eta}{r} d\eta \\ &= \sum_{t=0}^{2^s-1} \left(\frac{\ell}{\sqrt{k}}\right)^{N-\vec{n}\cdot\vec{t}} \left(\frac{d}{\sqrt{h}}\right)^{\vec{n}\cdot\vec{t}} \left(\prod_{i=1}^{s} C_i^{1-t_i} \right) \frac{1}{r} \\ &\times \int_{-\infty}^{+\infty} \sin^{N-\vec{t}\cdot\vec{n}} \left(\frac{\eta \ell}{K_b T}\right) \sin^{\vec{t}\cdot\vec{n}} \left(\frac{\eta d}{K_b T}\right) \sin\left(\frac{\eta r}{K_b T}\right) \frac{1}{\eta^{N-1}} d\eta. \end{aligned} \tag{23}$$

The function to integrate in Equation (23) is regular on the real axis and analytical on a strip $|\Im\, \eta| < M$ of the complex plane, for an arbitrary $M \in \Re$. Then, instead of integrating on the whole real axis, we can use the path Γ shown in Figure 3. With the change of variable $y = \eta \ell / (K_b T)$, we then have

$$\begin{aligned} Z_H(r) &= -i \left(\frac{\ell}{K_b T}\right)^{N-2} \sum_{t=0}^{2^s-1} \left(\frac{\ell}{\sqrt{k}}\right)^{N-\vec{n}\cdot\vec{t}} \left(\frac{d}{\sqrt{h}}\right)^{\vec{n}\cdot\vec{t}} \left(\prod_{i=1}^{s} C_i^{1-t_i} \right) \\ &\times \frac{1}{r} \int_{\Gamma} \sin^{N-\vec{t}\cdot\vec{n}}(y) \sin^{\vec{t}\cdot\vec{n}} \left(\frac{d}{\ell} y\right) e^{i\frac{r}{\ell} y} \frac{1}{y^{N-1}} d\eta. \end{aligned} \tag{24}$$

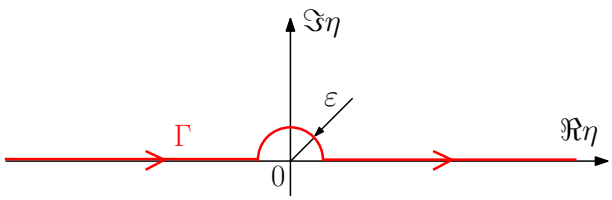

Figure 3. Definition of the contour Γ on the complex plane.

By developing the powers of trigonometric functions in the previous expression by means of the expansion [68,70,74]

$$\sin^m y = \frac{1}{(2i)^m} e^{imy} \sum_{t=0}^{m} \binom{m}{t} (-1)^t e^{-2ity}, \tag{25}$$

and by using the integral [68,70,74]

$$\int_\Gamma \frac{e^{iay}}{y^m} dy = \begin{cases} 0 & \text{if} \quad a > 0 \\ -2\pi i^m \frac{a^{m-1}}{(m-1)!} & \text{if} \quad a \leq 0 \end{cases}, \tag{26}$$

after straightforward calculations, we obtain the final result

$$\begin{aligned} Z_H(r) \quad = \quad & c \sum_{t=0}^{2^s-1} \left(\frac{\ell}{\sqrt{k}}\right)^{N-\vec{n}\cdot\vec{t}} \left(\frac{d}{\sqrt{h}}\right)^{\vec{n}\cdot\vec{t}} \left(\prod_{i=1}^{s} C_i^{1-t_i}\right) \frac{1}{r} \\ & \times \sum_{p=0}^{N-\vec{n}\cdot\vec{t}} \sum_{q=0}^{\vec{n}\cdot\vec{t}} \binom{N-\vec{n}\cdot\vec{t}}{p} \binom{\vec{n}\cdot\vec{t}}{q} (-1)^{p+q} \\ & \times \left(N - \vec{n}\cdot\vec{t} - 2p + \frac{d}{\ell}\vec{n}\cdot\vec{t} - \frac{2qd}{\ell} + \frac{r}{\ell}\right)^{N-2} \\ & \times \mathbf{1}\left(-N + \vec{n}\cdot\vec{t} + 2p - \frac{d}{\ell}\vec{n}\cdot\vec{t} + \frac{2qd}{\ell} - \frac{r}{\ell}\right), \end{aligned} \tag{27}$$

where $c = \frac{\pi}{2(N-2)!}\left(\frac{l}{2K_bT}\right)^{N-2}$ is an irrelevant multiplicative constant and the Heaviside step function $\mathbf{1}(x)$ is defined as $\mathbf{1}(x) = 1$ if $x \geq 0$, and $\mathbf{1}(x) = 0$ if $x < 0$. This is the final result describing the thermoelasticity of the ideal chain with sacrificial bonds under the isometric Helmholtz condition.

The knowledge of the partition function allows us to obtain the force–extension response within the Helmholtz ensemble through the expression [32,41]

$$\langle f \rangle = -k_B T \frac{\partial \log Z_H(r)}{\partial r}, \tag{28}$$

which will be used to discuss the behavior of the system with the prescribed extension. In particular, it will be adopted to show the characteristic sawtooth pattern and to evaluate the extra-toughness.

An interesting point concerning the thermomechanics of polymeric chains is the equivalence of the ensembles in the thermodynamic limit (i.e., for $N \to \infty$) [41,78–81]. Two conjugated ensembles (for instance, the Gibbs and Helmholtz ones) are said to be equivalent when the macroscopic behavior described by the force–extension relation is the same for $N \to \infty$. In general, it is difficult to prove for a given system if two statistical ensembles are equivalent. Although there are some particular rules, there are no general criteria or theorems for determining whether a system satisfies such an equivalence [80]. Several examples of non-equivalence are well-known in the literature [82–87]. However, in our system, which is a generalization of the extensible freely-jointed chain [69], it is not difficult to prove that the equivalence of the ensembles in the thermodynamic limit is verified.

3. Results and Discussion

Here, we present some examples of applications of previous results in order to better understand the role of the different parameters of the system on the mechanical performances (particularly on the extra-toughness). The force–extension curves were obtained by the implementation of Equations (15) and (21) for the Gibbs ensemble and of Equations (27) and (28) for the Helmholtz ensemble. While the partition functions have been implemented in closed

form, the derivatives to obtain the averaged macroscopic quantities have been calculated numerically. It is important to observe that if we plot the force–extension curves in terms of the adimensional force $f\ell/(K_bT)$ and adimensional extension $r/(N\ell)$, then the curve only depends on the adimensional parameters d/ℓ, h/k, n_j and $E_j/(K_bT)$, $\forall j = 1, ..., s$. We should also note that in all of the following plots we have written the quantities $f\ell/(K_bT)$ and $r/(N\ell)$ on the two axes. However, this is not very accurate in that we should have written $f\ell/(K_bT)$ and $\langle r\rangle/(N\ell)$ for the Gibbs ensemble and $\langle f\rangle\ell/(K_bT)$ and $r/(N\ell)$ for the Helmholtz ensemble. The choice comes only from the fact that we superimposed the two curves in the same graph. We leave correct interpretation of the axes to the reader.

To begin, in Figure 4, we show the mechanical response of a chain with only one sacrificial bond (left panel) and with $s = 5$ sacrificial bonds (right panel) under both Gibbs (blue curves) and Helmholtz (red curves) conditions. In addition, the green curves correspond to the case of a chain without sacrificial bonds. The sacrificial bonds are homogeneous, i.e., with the same length and fracture energy. On the left panel, we observe that the rupture of the sacrificial bond corresponds to a force plateau in the Gibbs ensemble, representing the releasing of the hidden length. In the same panel, we also note that the Helmholtz response is described by a peak of force in the same region of the Gibbs plateau. The same behavior can be observed on the right panel where we see one plateau for the Gibbs response and five force peaks for the Helmholtz response. It means that in the Gibbs case the ruptures are synchronized when the force reaches a given threshold value. In contrast, in the Helmholtz case, breaks occur sequentially as the chain extension progresses continuously. The synchronized versus sequential transitions are well known in the protein folding/unfolding process [68]. The value of the plateau force in the Gibbs ensemble turns out to be temperature independent, as already observed in other investigations [68,69,72–75]. This result can be simply explained in the framework of the Bell relation $f = E/\Delta r$, discovered in the context of cell adhesion [88,89], where Δr is the hidden length in our system. This plateau force can be explained as follows. We consider two potential energies $U_1(r) = \frac{1}{2}k(r - nd)^2 - fr$ and $U_2(r) = E + \frac{1}{2}k(r - n\ell)^2 - fr$, corresponding to the intact and broken states of one sacrificial bond under force f, when $h/k = 1$. In both cases, the equilibrium lengths are defined by $\partial U_1/\partial r = 0$ and $\partial U_2/\partial r = 0$, and we obtain $r_1 = nd + f/k$ and $r_2 = n\ell + f/k$. Finally, the broken configuration is more favorable than the intact one when $U_2(r_2) < U_1(r_1)$, which corresponds to $f > f^* = E/\Delta x$, with $\Delta x = n(\ell - d)$ being the hidden length of the bond. This force plateau value can be written in an adimensional form as $f^*\ell/(K_bT) = \frac{1}{n}\frac{E}{K_bT}\frac{1}{1-d/\ell}$, perfectly corresponding with the values in Figure 4. The previous argument can be easily generalized also for the case with $k \neq h$, but let us skip this detail for the sake of brevity. We see that the introduction of the sacrificial bonds increases the toughness of the system. This improvement can be measured quantitatively by means of the following definition of the extra-toughness

$$\mathcal{E} = \frac{1}{NK_bT}\int_0^{+\infty}[f_s(r) - f_0(r)]dr, \tag{29}$$

where $f_s(r)$ is the force–extension curve with s sacrificial bonds and $f_0(r)$ is the same curve without sacrificial bonds. For the Gibbs case, it corresponds to the area between the blue and green curves, divided by K_bT. Similarly, for the Helmholtz case, it corresponds to the area between the red and green curves, divided by K_bT. The integral always converges since $f_s(r) \sim f_0(r)$ for $r \to \infty$ (when all sacrificial bonds are broken). In the following, we will evaluate this quantity for the Helmholtz condition, which is the most widely used in this type of analysis (the integral will be performed numerically).

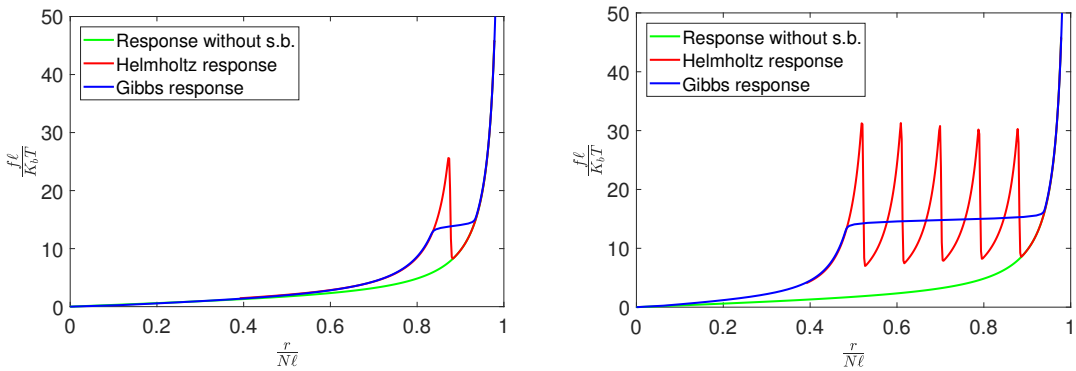

Figure 4. Force–extension response of a chain with only one sacrificial bond (left panel) and with $s = 5$ sacrificial bonds (right panel) under both Gibbs (blue curves) and Helmholtz (red curves) conditions. We also added the response of the same system without sacrificial bonds in order to compare the different behaviors (green curves). The plots are represented with adimensional quantities. We adopted the parameters $N = 50$, $h/k = 1$, $d/\ell = 1/10$, $n = 5$ and $E/(K_bT) = 75$ for all sacrificial bonds.

In Figure 5, we show two examples of force–extension curves with two kinds of distribution of heterogeneous sacrificial bonds. On the left panel, we have a heterogeneous distribution of lengths but a homogeneous distribution of fracture energies ($n_k = k\forall k$ and $E_k/(K_bT) = 75\forall k$). Conversely, on the right panel, we have a homogeneous distribution of lengths but a heterogeneous distribution of fracture energies ($n_k = 5\forall k$ and $E_k/(K_bT) = 35k\forall k$). We note that in this case with heterogeneous distributions of sacrificial bonds, we have in the Gibbs response a multi-plateau pattern where each plateau corresponds to the threshold force for breaking a given sacrificial bond. Indeed, we could repeat the previous argument in order to obtain the expression $f_k^*\ell/(K_bT) = \frac{1}{n_k}\frac{E_k}{K_bT}\frac{1}{1-d/\ell}$, giving the adimensional form of the threshold force for a given sacrificial bond, with length n_k and fracture energy E_k. It is possible to verify that this simple result perfectly corresponds with the plateau values in Figure 5. It can be seen from these examples that the sawtooth curve of the response in the Helmholtz case is strongly dependent on the distribution of sacrificial bonds. Before analyzing how extra-toughness varies as different parameters change, let us look at a few more examples.

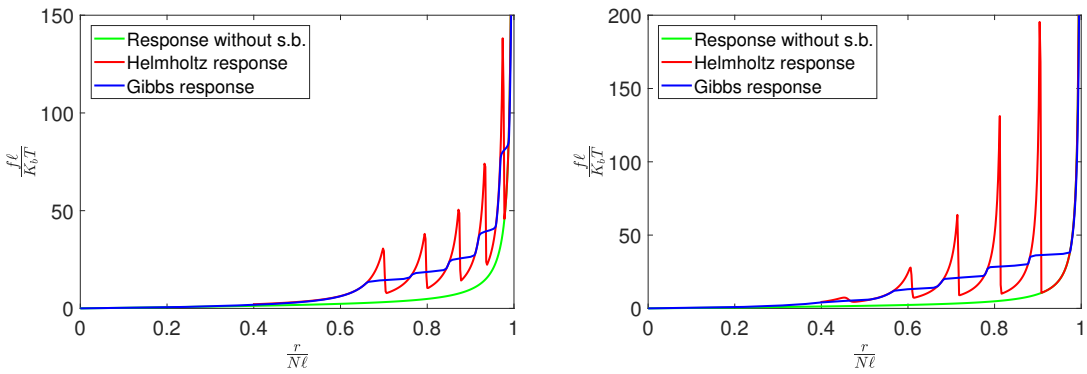

Figure 5. Force–extension response of two chains with $s = 5$ and different heterogeneous distributions of sacrificial bonds under both Gibbs (blue curves) and Helmholtz (red curves) conditions. We also added the response of the same system without sacrificial bonds in order to compare the different behaviors (green curves). On the left panel, we assumed $n_k = k\forall k$ and $E_k/(K_bT) = 75\forall k$, while on the right panel we adopted $n_k = 5\forall k$ and $E_k/(K_bT) = 35k\forall k$. The plots are represented with adimensional quantities. The other parameters are given by $N = 50$, $h/k = 1$, and $d/\ell = 1/10$.

Since the adimensional threshold forces are given by $f_k^* \ell/(K_b T) = \frac{1}{n_k} \frac{E_k}{K_b T} \frac{1}{1-d/\ell}$, it is possible to have a heterogeneous distribution of sacrificial bonds (but with a homogeneous distribution of threshold forces). It is sufficient to set all fractions $\frac{E_k}{n_k}$ to the same value. Two examples following this criterion can be found in Figure 6. On the left panel, we considered a chain with $s = 3$ and we assumed $n_k = 3 + k \forall k$ and $E_k/(K_b T) = 35 n_k \forall k$, while on the right panel, we analyzed a chain with $s = 4$ and we adopted $n_k = 3 + k \forall k$ and $E_k/(K_b T) = 30 n_k \forall k$. We clearly observe that in these two cases the Gibbs response is described by a single plateau that corresponds to the synchronized breaking of all sacrificial bonds. In fact, the threshold-breaking strength is the same for all sacrificial bonds. We move then from the multi-plateau case to the single plateau case. However, the Helmholtz ensemble is more complicated since, in addition to the s main force peaks, we note the emergence of some smaller force peaks. The origin of such minor peaks can be explained as follows. If we look at the curves in Figure 5 and imagine deforming them in order to bring all the Gibbs plateaus to the same level, we see that in the Helmholtz curves we have to make a folding that generates exactly the minor peaks observable in Figure 6. From the physical point of view, it means that there is an interaction between the rupture process of the different sacrificial bonds. This fact is consistent with the general principle that in the Helmholtz ensemble the chain segments are not independent because the constraint on the total extension creates an implicit interaction between them (the distance between the ends is fixed) [68]. In contrast, in the Gibbs ensemble, they are always independent because the application of force does not create constraints between the chain segments [68]. From the point of view of statistical mechanics, this fact is evident from the structure of the partition function: in the Gibbs ensemble, it is given by the product of the partial functions of the segments, see Equation (15), while this simple form cannot be identified for the Helmholtz ensemble, see Equation (27).

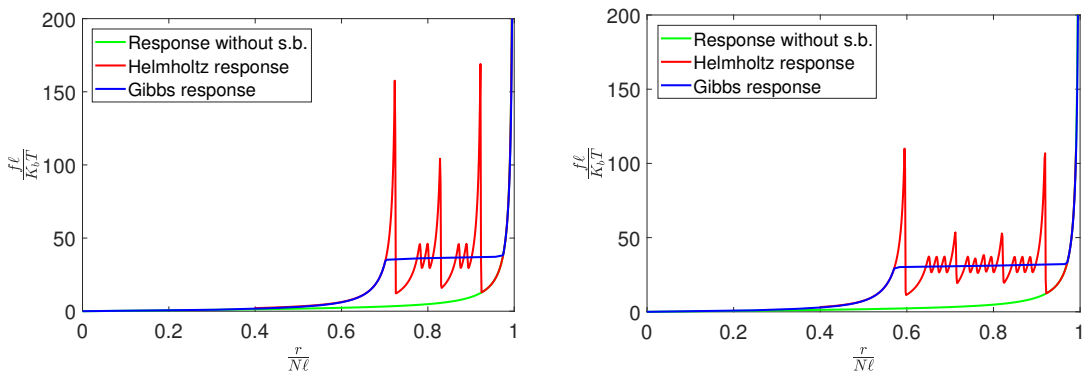

Figure 6. Force–extension response of two chains with $s = 3$ (left panel) and $s = 4$ (right panel) and different heterogeneous distributions of sacrificial bonds under both Gibbs (blue curves) and Helmholtz (red curves) conditions. We also added the response of the same system without sacrificial bonds in order to compare the different behaviors (green curves). On the left panel, we assumed $n_k = 3 + k \forall k$ and $E_k/(K_b T) = 35 n_k \forall k$, while on the right panel, we adopted $n_k = 3 + k \forall k$ and $E_k/(K_b T) = 30 n_k \forall k$. The plots are represented with adimensional quantities. The other parameters are given by $N = 50$, $h/k = 1$, and $d/\ell = 1/10$.

We now begin to analyze the behavior of extra-toughness as the system parameters change. We start with the simple case in which there is only one sacrificial bond with a variable braking energy. The results can be found in Figure 7. On the left panel, one can find the different force–extension curves with an increasing rupture energy E, while in the right panel, we plot the extra-toughness $\mathcal{E}$ defined in Equation (29) versus $E_k/(K_b T)$. Of course, we observe an increasing extra-toughness with increasing braking energy. Nevertheless, it is interesting to note that there is a threshold value of energy below which extra-toughness is zero, and beyond this value, the behavior is perfectly linear.

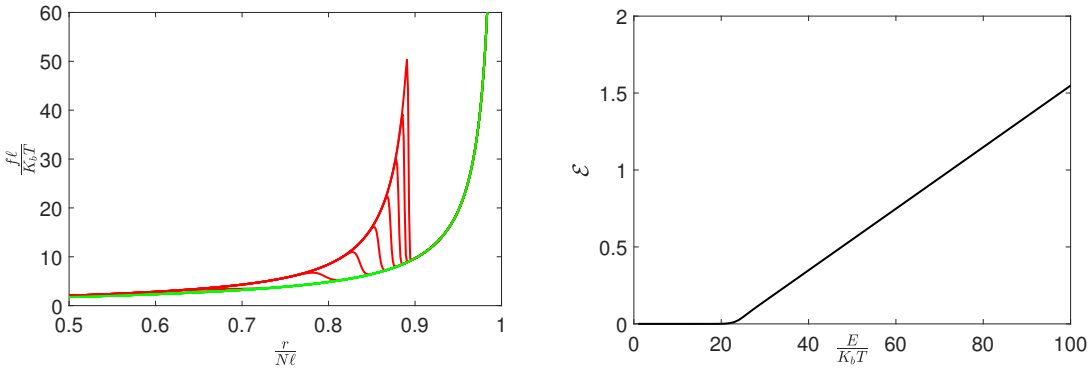

Figure 7. Helmholtz force–extension response (left panel, red curves) and extra-toughness (right panel, black curve) for a chain with $s = 1$ and $n = 5$ and an increasing value of the rupture energy E. We also added the response of the same system without sacrificial bonds in order to compare the different behaviors (green curve). On the left panel, we assumed $E/(K_bT) = 10, 20, 30, 40, 50, 60, 70, 80, 90, 100$, while on the right panel, we varied $E_k/(K_bT)$ continuously between 0 and 100. The plots are represented with adimensional quantities. The other parameters are given by $N = 50$, $h/k = 1$, and $d/\ell = 1/10$.

In Figure 8, we found the behavior of the extra-toughness in terms of the sacrificial bond length. We consider a simple chain with only one sacrificial bond and we vary n from 1 to 10, by keeping the other parameters constant. We see that the extra-toughness is a linearly decreasing function of n. This behavior can be explained by observing that since the Gibbs plateau is given by the formula $f^*\ell/(K_bT) = \frac{1}{n}\frac{E}{K_bT}\frac{1}{1-d/\ell}$, we see that it is inversely proportional to n and, therefore, the area subtended by the curve is also decreasing with n. The same argument is clearly also valid for the Helmholtz peak, which is related to the Gibbs plateau. We deduce that short sacrificial bonds are more efficient for improving the system toughness. This behavior has been obtained by considering a constant value of the rupture energy E for any value of n.

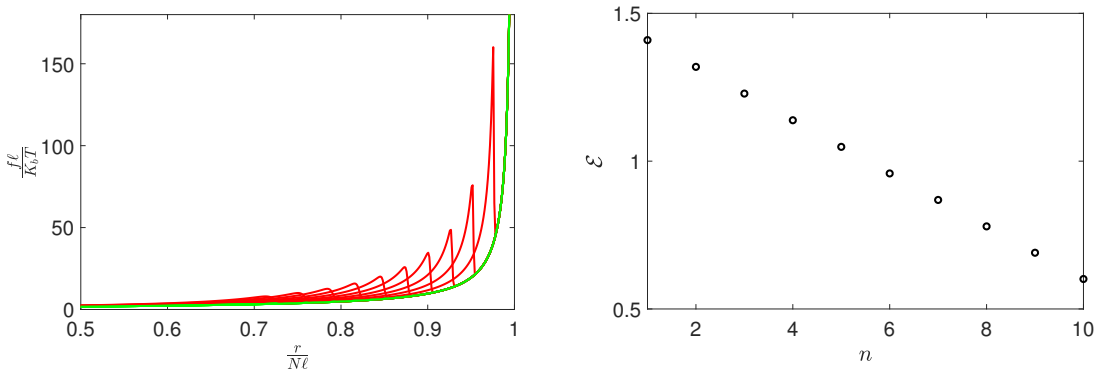

Figure 8. Helmholtz force–extension response (left panel, red curves) and extra-toughness (right panel, black symbols) for a chain with $s = 1$ and an increasing length n of the sacrificial bond. We also added the response of the same system without sacrificial bonds in order to compare the different behaviors (green curve). We assumed $n = 1, 2, 3, ..., 10$. The plots are represented with adimensional quantities. The other parameters are given by $N = 50$, $h/k = 1$, $E/(K_bT) = 75$ and $d/\ell = 1/10$.

Differently, in Figure 9, we consider again only one sacrificial bond but we assume that the rupture energy is proportional to the bond length. In particular, we suppose that $n = 1, 2, 3, ..., 10$ and the corresponding rupture energies are given by $E/(K_bT) = 20n$. In this case, in contrast to the previous one, we see that longer sacrificial bonds are more efficient from the point of view of the extra-toughness. This example shows the complexity of the system and teaches us that the rupture energies are crucial in determining the toughness of the system.

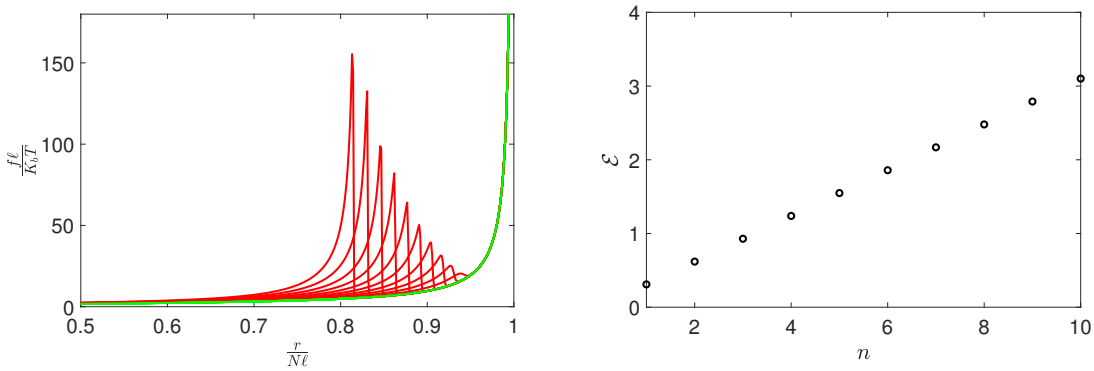

Figure 9. Helmholtz force–extension response (left panel, red curves) and extra-toughness (right panel, black symbols) for a chain with $s = 1$, an increasing length n of the sacrificial bond, and rupture energy proportional to the length. We also added the response of the same system without sacrificial bonds in order to compare the different behaviors (green curves). We assumed $n = 1, 2, 3, ..., 10$ and the corresponding rupture energies are given by $E/(K_bT) = 20n$. The plots are represented with adimensional quantities. The other parameters are given by $N = 50$, $h/k = 1$, and $d/\ell = 1/10$.

We studied the effects of the length n, and now we can analyze those of the number s of sacrificial bonds. The results can be seen in Figure 10, where we studied the extra-toughness by varying both s and n. We consider here a homogeneous distribution of sacrificial bonds. While on the left panel we represented the force–extension curves for different values of s with a fixed length n, on the right panel we show the values of the extra-toughness $\mathcal{E}$ versus the number s of sacrificial bonds, by taking n as a parameter. Importantly, we observe that the extra-toughness is a linearly increasing function of the number s of sacrificial bonds, and it is a slightly decreasing function of the length n, as predicted by Figure 8. It is clear that the number of sacrificial bonds is the key parameter to focus on in order to increase the toughness of the system.

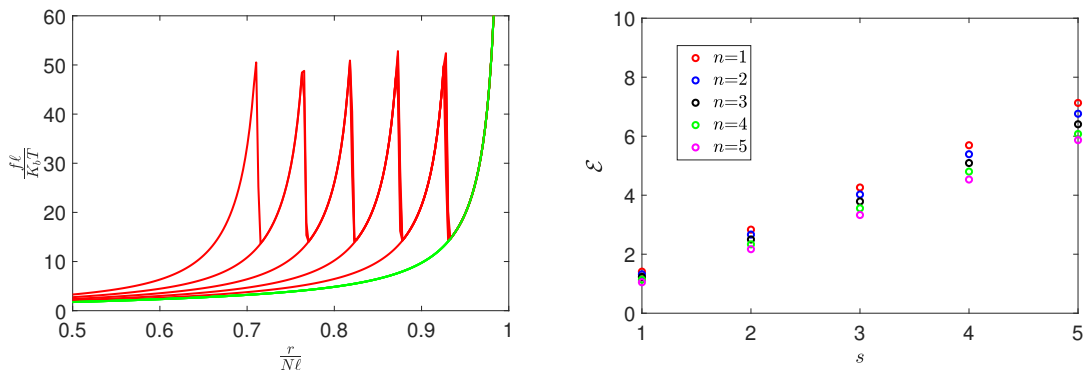

Figure 10. Helmholtz force–extension response (left panel, red curves) and extra-toughness (right panel, colored symbols) for a chain with different s and n. We also added the response of the same system without sacrificial bonds in order to compare the different behaviors (green curve). On the left panel, we considered a chain with $s = 1, ..., 5$ with the fixed value $n = 3$. On the right panel, the extra-toughness is calculated for $n = 1, ..., 5$ and $n = 1, ..., 5$. The plots are represented with adimensional quantities. The other parameters are given by $N = 50$, $h/k = 1$, $E/(K_bT) = 75$, and $d/\ell = 1/10$.

Another analysis concerns the effect of the length ratio d/ℓ on the extra-toughness. In Figure 11, one can find on the left panel three different force–extension curves characterized by different ratios $d/\ell = 1/10, 3/10, 1/2$ (pink, brown, and red curves, respectively), and on the right panel, the behavior of $\mathcal{E}$ versus d/ℓ for different values of s and n. In general, we observe a slightly increasing trend of $\mathcal{E}$, which can be justified again by the expression $f_k^*\ell/(K_bT) = \frac{1}{n_k}\frac{E_k}{K_bT}\frac{1}{1-d/\ell}$, giving the adimensional force plateau for a given sacrificial

bond. Indeed, we can see that this value increases as d/ℓ increases and, thus, the areas under both the Gibbs and Helmholtz curves increase with d/ℓ as well. However, the variation in extra-toughness is not very large. Moreover, in fact, in real physical systems, the sacrificial bonds are much shorter than the short-circuited sections of the main chain for other chemical–physical reasons. In fact, such sacrificial links are often driven by chemical bonds that are weaker than the covalent bond and, thus, have limited extension.

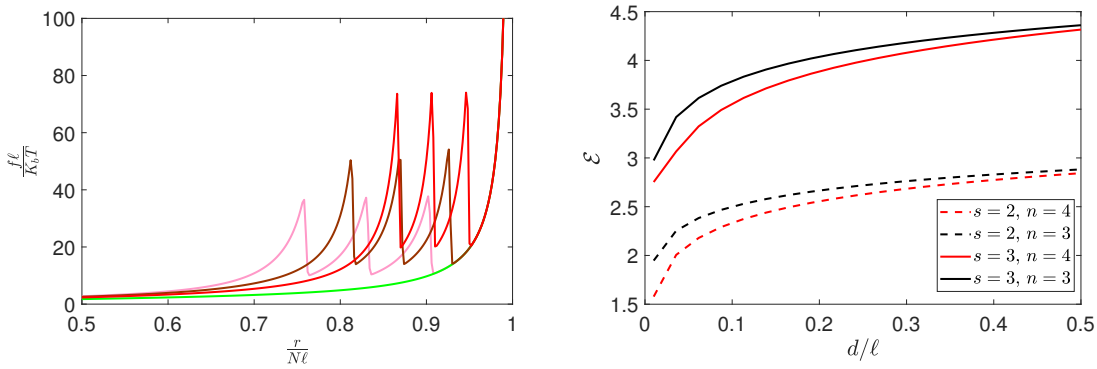

Figure 11. Helmholtz force–extension response (left panel) and extra-toughness (right panel) for a chain with different s and n and varying d/ℓ. We also added the response of the same system without sacrificial bonds in order to compare the different behaviors (green curve). On the left panel, we considered a chain with $s = 3$, $n = 4$ and $d/\ell = 1/10, 3/10, 1/2$ (pink, brown, and red curves, respectively). On the right panel, the extra-toughness is calculated for $n = 3, 4$, $s = 2, 3$ and $1/100 < d/\ell < 1/2$. The plots are represented with adimensional quantities. The other parameters are given by $N = 50$, $h/k = 1$, and $E/(K_bT) = 75$.

In Figure 12, we also investigated the variation of the extra-toughness in terms of the elastic constants ratio h/k for chains with different geometries. We considered a chain with $s = 3$, $n = 2, 3, 4$ (red, black, and blue curves, respectively), and we varied h/k in the interval (0,1) on the left panel, and the interval (1,10) on the right panel. We can directly infer that extra-toughness increases as the ratio h/k decreases. This is consistent with the fact that sacrificial bonds are weak and typically have a lower elastic constant than the main chain.

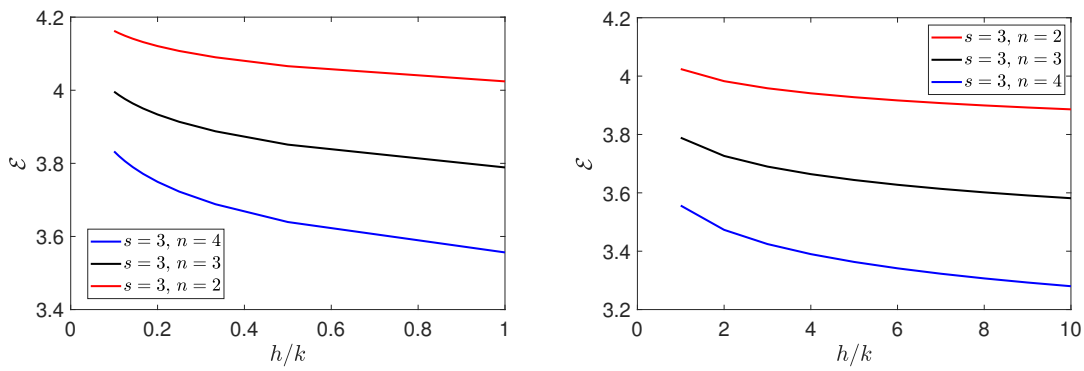

Figure 12. Extra-toughness $\mathcal{E}$ behavior versus the elastic constants ratio h/k for chains with different geometries. We considered a chain with $s = 3$, $n = 2, 3, 4$ (red, black, and blue curves, respectively) and we varied h/k in the interval (0,1) on the left panel, and in the interval (1,10) on the right panel. The plots are represented with adimensional quantities. The other parameters are given by $N = 50$, $d/\ell = 1/10$, and $E/(K_bT) = 75$.

To conclude, we performed an analysis concerning the stochastic behavior of the system. In particular, we considered a chain with a given distribution and geometry of sacrificial bonds, but we assumed that the rupture energies were random variables. The results of this further study are represented in Figure 13. All rupture energies (normalized,

i.e., $\frac{E}{K_bT}$) were generated by means of independent translated exponential distributions described by the probability density

$$f_X(x) = \frac{1}{\mu} e^{-\frac{x-\lambda}{\mu}}, x \geq \lambda, \tag{30}$$

with μ and λ, two real parameters, we suppose that $f_E(x) = 0$ when $x < \lambda$. This probability density is characterized by the average value

$$\langle X \rangle = \int_{\lambda}^{+\infty} e f_E(x) dx = \mu + \lambda, \tag{31}$$

and by a variance

$$\sigma_X^2 = \left\langle (X - \langle X \rangle)^2 \right\rangle = \int_{\lambda}^{+\infty} (x - \langle X \rangle)^2 f_E(x) dx = \mu^2. \tag{32}$$

From these relations, we can write $\lambda = \langle X \rangle - \sigma_X$ and $\mu = \sigma_X$. On the left panel, we assumed an independent exponential distribution of the rupture energies with a fixed average value and varying variance. More precisely, we assumed $\left\langle \frac{E}{K_bT} \right\rangle = 60$, and $\sigma_{\frac{E}{K_bT}}$ variable between 1 and 40. Conversely, on the right panel, we assumed an independent exponential distribution of the rupture energies with fixed variance and varying average value. We assumed $\sigma_{\frac{E}{K_bT}} = 40$, and $\left\langle \frac{E}{K_bT} \right\rangle$ varying between 30 and 100. From the left panel, we deduce that the variance of the rupture energies does not affect the extra-toughness since $\mathcal{E}$ remains quite constant over a large range of $\sigma^2_{\frac{E}{K_bT}}$. Moreover, we see on the right panel that the extra-toughness $\mathcal{E}$ increases linearly with $\left\langle \frac{E}{K_bT} \right\rangle$ when the variance is constant. This is the same behavior already observed in Figure 7 for a deterministic system. The important conclusion is that the statistical distribution of the rupture energies does not affect the system behavior and only the average value of these quantities can induce a marked improvement of the mechanical performances.

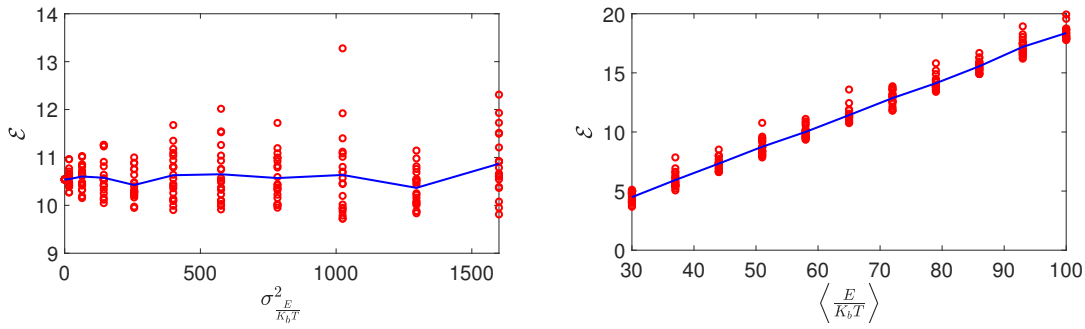

Figure 13. Extra-toughness behavior $\mathcal{E}$ in terms of the stochastic distribution of sacrificial bond rupture energies. In both examples, we considered a chain with $s = 4$ and $n = 2$. On the left panel, we assumed an independent exponential distribution of the rupture energies with a fixed average value and varying variance. Conversely, on the right panel, we assumed an independent exponential distribution of the rupture energies with fixed variance and varying average value (see details in the main text). The red circles represent the single results (Monte Carlo realizations) and the blue lines the corresponding average values. The other parameters are given by $N = 20$, $h/k = 1$, and $d/\ell = 1/10$.

4. Conclusions

We developed a simple model, based on statistical mechanics and thermodynamics of the elastic behavior of a polymeric chain or macromolecule with sacrificial bonds. The model takes into account the hidden length and the resulting extra-toughness, which are the two main ingredients used by biological structures to create high-toughness and

high-performance materials. The approach is based on the spin variable methods, where discrete quantities, such as bits, are introduced to identify the state (intact or broken) of the sacrificial bonds during the load application. It allows the determination of the force–extension relation of the chain under both Gibbs (with applied force) and Helmholtz (with prescribed extension) conditions. The knowledge of this force–extension relation permits obtaining the characteristic sawtooth pattern observed in force spectroscopy experiments and evaluating the extra-toughness generated by the sacrificial bonds system. The model, while simple, was developed (exactly and analytically) from reasonable assumptions. Thus, it allows for studying the effect of key parameters on macromolecular chain performance. We showed some examples in this regard, to analyze the behavior of the system, as the lengths of the chain elements, breaking energies, sacrificial bond geometry, and so on, vary. However, the model can be generalized in a variety of directions to be more closely tailored to the chemical and physical realities of biological structures. First, we used a generalization of the FJC model that did not allow for the introduction of a persistence length in the chains. This point can be remedied by the use of the WLC model, which is more mathematically complex and, therefore, does not allow for an easy focus on issues related to sacrificial bonds [43–46]. In addition, we approached the problem with statistical mechanics at equilibrium, so the results are valid only for static or quasi-static processes, as in classical thermodynamics. Consideration of dynamics would be an important point to take into account the true traction velocities used in force spectroscopy experiments. Typical values in AFM force-spectroscopy experiments range between 10^{-2} and 10^{2} μm/s [90] (only recently, high-speed atomic force microscopes HS-AFM attained speeds of about 10^{4} μm/s [91]). In order to take this issue into consideration, the equilibrium statistical mechanics approaches should be substituted with the methodologies based on the Langevin and Fokker–Planck stochastic formalism [92–95]. Moreover, other limitations concern the geometry of the system. First of all, we developed our model only for a single chain, but in real systems, the material toughness depends on a complex interaction among many chains coexisting in a given structure (rubber-like materials). In addition, we considered only sacrificial links that did not overlap and interact with each other in the simple chain. These structural and geometric limitations should also be reduced with more complex modeling that would probably have to be studied entirely numerically.

Author Contributions: Conceptualization, methodology, supervision, S.G.; software, formal analysis, investigation, S.G. and R.J.D.M.; writing—original draft preparation, writing—review and editing, S.G. and R.J.D.M. All authors have read and agreed to the published version of the manuscript.

Funding: This research received no external funding.

Institutional Review Board Statement: Not applicable.

Informed Consent Statement: Not applicable.

Data Availability Statement: Not applicable.

Conflicts of Interest: The authors declare no conflict of interest.

Abbreviations

The following abbreviations are used in this manuscript:

AFM	atomic force microscope
HS-AFM	high speed atomic force microscope
MEMS	microelectromechanical systems
NEMS	nanoelectromechanical systems
CDN	composite double network
FJC	freely-jointed chain
WLC	worm-like chain
DNA	deoxyribonucleic acid
RNA	ribonucleic acid

References

1. Cranford, S.W.; Buehler, M.J. *Biomateriomics*, 2012nd ed.; Springer: Dordrecht, The Netherlands, 2014; ISBN 9789400796867.
2. Smith, B.L.; Schäffer, T.E.; Viani, M.; Thompson, J.B.; Frederick, N.A.; Kindt, J.; Belcher, A.; Stucky, G.D.; Morse, D.E.; Hansma, P.K. Molecular Mechanistic Origin of the Toughness of Natural Adhesives, Fibres and Composites. *Nature* **1999**, *399*, 761–763. [CrossRef]
3. Fantner, G.E.; Oroudjev, E.; Schitter, G.; Golde, L.S.; Thurner, P.; Finch, M.M.; Turner, P.; Gutsmann, T.; Morse, D.E.; Hansma, H.; et al. Sacrificial Bonds and Hidden Length: Unraveling Molecular Mesostructures in Tough Materials. *Biophys. J.* **2006**, *90*, 1411–1418. [CrossRef] [PubMed]
4. Nabavi, S.S.; Harrington, M.J.; Fratzl, P.; Hartmann, M.A. Influence of Sacrificial Bonds on the Mechanical Behaviour of Polymer Chains. *Bioinspired Biomim. Nanobiomaterials* **2014**, *3*, 139–145. [CrossRef]
5. Soran Nabavi, S.; Harrington, M.J.; Paris, O.; Fratzl, P.; Hartmann, M.A. The Role of Topology and Thermal Backbone Fluctuations on Sacrificial Bond Efficacy in Mechanical Metalloproteins. *New J. Phys.* **2014**, *16*, 013003. [CrossRef]
6. Lieou, C.K.C.; Elbanna, A.E.; Carlson, J.M. Sacrificial Bonds and Hidden Length in Biomaterials: A Kinetic Constitutive Description of Strength and Toughness in Bone. *Phys. Rev. E Stat. Nonlin. Soft Matter Phys.* **2013**, *88*, 012703. [CrossRef] [PubMed]
7. Elbanna, A.E.; Carlson, J.M. Dynamics of Polymer Molecules with Sacrificial Bond and Hidden Length Systems: Towards a Physically-Based Mesoscopic Constitutive Law. *PLoS ONE* **2013**, *8*, e56118. [CrossRef]
8. Fantner, G.E.; Hassenkam, T.; Kindt, J.H.; Weaver, J.C.; Birkedal, H.; Pechenik, L.; Cutroni, J.A.; Cidade, G.A.G.; Stucky, G.D.; Morse, D.E.; et al. Sacrificial Bonds and Hidden Length Dissipate Energy as Mineralized Fibrils Separate during Bone Fracture. *Nat. Mater.* **2005**, *4*, 612–616. [CrossRef]
9. Burr, D.B. The Contribution of the Organic Matrix to Bone's Material Properties. *Bone* **2002**, *31*, 8–11. [CrossRef]
10. Thompson, J.B.; Kindt, J.H.; Drake, B.; Hansma, H.G.; Morse, D.E.; Hansma, P.K. Bone Indentation Recovery Time Correlates with Bond Reforming Time. *Nature* **2001**, *414*, 773–776. [CrossRef] [PubMed]
11. Koebley, S.R.; Vollrath, F.; Schniepp, H.C. Toughness-Enhancing Metastructure in the Recluse Spider's Looped Ribbon Silk. *Mater. Horiz.* **2017**, *4*, 377–382. [CrossRef]
12. Thormann, E.; Mizuno, H.; Jansson, K.; Hedin, N.; Fernández, M.S.; Arias, J.L.; Rutland, M.W.; Pai, R.K.; Bergström, L. Embedded Proteins and Sacrificial Bonds Provide the Strong Adhesive Properties of Gastroliths. *Nanoscale* **2012**, *4*, 3910–3916. [CrossRef] [PubMed]
13. Fratzl, P.; Weinkamer, R. Nature's hierarchical materials. *Prog. Mater. Sci.* **2007**, *52*, 12631334. [CrossRef]
14. Gao, H. ;Ji, B.; Jäger, I.L.; Arzt, E.; Fratzl, P. Materials become insensitive to flaws at nanoscale: Lessons from nature. *Proc. Natl. Acad. Sci. USA* **2003**, *100*, 5597–5600. [CrossRef] [PubMed]
15. Manca, F.; Palla, P. L.; Cleri, F.; Giordano, S. Characteristic lengths in natural bundle assemblies arising from fiber-matrix energy competition: A Floquet-based homogenization theory. *Eur. J. Mech. A/Solids* **2016**, *60*, 145–165. [CrossRef]
16. Zhou, X.; Guo, B.; Zhang, L.; Hu, G.-H. Progress in Bio-Inspired Sacrificial Bonds in Artificial Polymeric Materials. *Chem. Soc. Rev.* **2017**, *46*, 6301–6329. [CrossRef]
17. Shabbir, H.; Dellago, C.; Hartmann, M.A. A High Coordination of Cross-Links Is Beneficial for the Strength of Cross-Linked Fibers. *Biomimetics* **2019**, *4*, 12. [CrossRef] [PubMed]
18. Jiang, Z.; Bhaskaran, A.; Aitken, H.M.; Shackleford, I.C.G.; Connal, L.A. Using Synergistic Multiple Dynamic Bonds to Construct Polymers with Engineered Properties. *Macromol. Rapid Commun.* **2019**, *40*, e1900038. [CrossRef] [PubMed]
19. Mazzotta, M.G.; Putnam, A.A.; North, M.A.; Wilker, J.J. Weak Bonds in a Biomimetic Adhesive Enhance Toughness and Performance. *J. Am. Chem. Soc.* **2020**, *142*, 4762–4768. [CrossRef]
20. Wang, Z.; Xiang, C.; Yao, X.; Le Floch, P.; Mendez, J.; Suo, Z. Stretchable Materials of High Toughness and Low Hysteresis. *Proc. Natl. Acad. Sci. USA* **2019**, *116*, 5967–5972. [CrossRef]
21. Zhang, Z.; Liu, J.; Li, S.; Gao, K.; Ganesan, V.; Zhang, L. Constructing Sacrificial Multiple Networks to Toughen Elastomer. *Macromolecules* **2019**, *52*, 4154–4168. [CrossRef]
22. Tang, Z.; Huang, J.; Guo, B.; Zhang, L.; Liu, F. Bioinspired Engineering of Sacrificial Metal-Ligand Bonds into Elastomers with Supramechanical Performance and Adaptive Recovery. *Macromolecules* **2016**, *49*, 1781–1789. [CrossRef]
23. Huang, J.; Tang, Z.; Yang, Z.; Guo, B. Bioinspired Interface Engineering in Elastomer/Graphene Composites by Constructing Sacrificial Metal-Ligand Bonds. *Macromol. Rapid Commun.* **2016**, *37*, 1040–1045. [CrossRef] [PubMed]
24. Hussain, I.; Sayed, S.M.; Liu, S.; Oderinde, O.; Yao, F.; Fu, G. Glycogen-Based Self-Healing Hydrogels with Ultra-Stretchable, Flexible, and Enhanced Mechanical Properties via Sacrificial Bond Interactions. *Int. J. Biol. Macromol.* **2018**, *117*, 648–658. [CrossRef] [PubMed]
25. Sun, M.; Qiu, J.; Lu, C.; Jin, S.; Zhang, G.; Sakai, E. Multi-Sacrificial Bonds Enhanced Double Network Hydrogel with High Toughness, Resilience, Damping, and Notch-Insensitivity. *Polymers* **2020**, *12*, 2263. [CrossRef] [PubMed]
26. Lin, C.; Li, Z.; Lei, K.; Jia, H.; Yu, L.; Zheng, Z.; Wang, X. Bioinspired Tunable Sacrificial Bonds Endowing Tetra-PEG Based PU Hydrogel with Tunable Mechanical Properties, Shape-Memory, and Self-Healing Functions. *Macromol. Mater. Eng.* **2018**, *303*, 1700542. [CrossRef]
27. Myllymäki, T.T.T.; Lemetti, L.; Nonappa; Ikkala, O. Hierarchical Supramolecular Cross-Linking of Polymers for Biomimetic Fracture Energy Dissipating Sacrificial Bonds and Defect Tolerance under Mechanical Loading. *ACS Macro Lett.* **2017**, *6*, 210–214. [CrossRef] [PubMed]

28. Tu, Z.; Liu, W.; Wang, J.; Qiu, X.; Huang, J.; Li, J.; Lou, H. Biomimetic High Performance Artificial Muscle Built on Sacrificial Coordination Network and Mechanical Training Process. *Nat. Commun.* **2021**, *12*, 2916. [CrossRef] [PubMed]
29. Xiao, L.; Huang, J.; Wang, Y.; Chen, J.; Liu, Z.; Nie, X. Tung Oil-Based Modifier Toughening Epoxy Resin by Sacrificial Bonds. *ACS Sustain. Chem. Eng.* **2019**, *7*, 17344–17353. [CrossRef]
30. Chen, Y.; Sanoja, G.; Creton, C. Mechanochemistry Unveils Stress Transfer during Sacrificial Bond Fracture of Tough Multiple Network Elastomers. *Chem. Sci.* **2021**, *12*, 11098–11108. [CrossRef]
31. Ducrot, E.; Chen, Y.; Bulters, M.; Sijbesma, R.P.; Creton, C. Toughening Elastomers with Sacrificial Bonds and Watching Them Break. *Science* **2014**, *344*, 186–189. [CrossRef] [PubMed]
32. Weiner, J.H. *Statistical Mechanics of Elasticity*, 2nd ed.; Dover Publications: Mineola, NY, USA, 2003; ISBN 9780486422602.
33. Doi, M. *Introduction to Polymer Physics*; Clarendon Press: Oxford, UK, 1995; ISBN 9780198517726.
34. Kleinert, H. Path *Integrals in Quantum Mechanics, Statistics, and Polymer Physics*, 2nd ed.; World Scientific Publishing: Singapore, 1995; ISBN 9789810214722.
35. Ritort, F. Single-Molecule Experiments in Biological Physics: Methods and Applications. *J. Phys. Condens. Matter* **2006**, *18*, R531. [CrossRef] [PubMed]
36. Neuman, K.C.; Nagy, A. Single-Molecule Force Spectroscopy: Optical Tweezers, Magnetic Tweezers and Atomic Force Microscopy. *Nat. Methods* **2008**, *5*, 491–505. [CrossRef]
37. Kumar, S.; Li, M.S. Biomolecules under Mechanical Force. *Phys. Rep.* **2010**, *486*, 1–74. [CrossRef]
38. Hoffmann, T.; Dougan, L. Single Molecule Force Spectroscopy Using Polyproteins. *Chem. Soc. Rev.* **2012**, *41*, 4781–4796. [CrossRef] [PubMed]
39. Perret, G.; Lacornerie, T.; Manca, F.; Giordano, S.; Kumemura, M.; Lafitte, N.; Jalabert, L.; Tarhan, M.C.; Lartigau, E.F.; Cleri, F.; et al. Real-Time Mechanical Characterization of DNA Degradation under Therapeutic X-Rays and Its Theoretical Modeling. *Microsyst. Nanoeng.* **2016**, *2*, 16062. [CrossRef]
40. Petrosyan, R. Improved Approximations for Some Polymer Extension Models. *Rheol. Acta* **2017**, *56*, 21–26. [CrossRef]
41. Manca, F.; Giordano, S.; Palla, P.L.; Zucca, R.; Cleri, F.; Colombo, L. Elasticity of Flexible and Semiflexible Polymers with Extensible Bonds in the Gibbs and Helmholtz Ensembles. *J. Chem. Phys.* **2012**, *136*, 154906. [CrossRef] [PubMed]
42. Manca, F.; Giordano, S.; Palla, P.L.; Cleri, F.; Colombo, L. Theory and Monte Carlo Simulations for the Stretching of Flexible and Semiflexible Single Polymer Chains under External Fields. *J. Chem. Phys.* **2012**, *137*, 244907. [CrossRef] [PubMed]
43. Marko, J.F.; Siggia, E.D. Statistical Mechanics of Supercoiled DNA. *Phys. Rev. E Stat. Phys. Plasmas Fluids Relat. Interdiscip. Top.* **1995**, *52*, 2912–2938. [CrossRef] [PubMed]
44. Marko, J.F.; Siggia, E.D. Stretching DNA. *Macromolecules* **1995**, *28*, 8759–8770. [CrossRef]
45. Smith, S.B.; Cui, Y.; Bustamante, C. Overstretching B-DNA: The Elastic Response of Individual Double-Stranded and Single-Stranded DNA Molecules. *Science* **1996**, *271*, 795–799. [CrossRef] [PubMed]
46. Storm, C.; Nelson, P.C. Theory of High-Force DNA Stretching and Overstretching. *Phys. Rev. E Stat. Nonlin. Soft Matter Phys.* **2003**, *67*, 051906. [CrossRef] [PubMed]
47. Rief, M.; Fernandez, J.M.; Gaub, H.E. Elastically Coupled Two-Level Systems as a Model for Biopolymer Extensibility. *Phys. Rev. Lett.* **1998**, *81*, 4764–4767. [CrossRef]
48. Staple, D.B.; Payne, S.H.; Reddin, A.L.C.; Kreuzer, H.J. Stretching and Unfolding of Multidomain Biopolymers: A Statistical Mechanics Theory of Titin. *Phys. Biol.* **2009**, *6*, 025005. [CrossRef] [PubMed]
49. Prados, A.; Carpio, A.; Bonilla, L.L. Sawtooth Patterns in Force-Extension Curves of Biomolecules: An Equilibrium-Statistical-Mechanics Theory. *Phys. Rev. E Stat. Nonlin. Soft Matter Phys.* **2013**, *88*, 012704. [CrossRef] [PubMed]
50. Bonilla, L.L.; Carpio, A.; Prados, A. Theory of Force-Extension Curves for Modular Proteins and DNA Hairpins. *Phys. Rev. E Stat. Nonlin. Soft Matter Phys.* **2015**, *91*, 052712. [CrossRef] [PubMed]
51. De Tommasi, D.; Millardi, N.; Puglisi, G.; Saccomandi, G. An Energetic Model for Macromolecules Unfolding in Stretching Experiments. *J. R. Soc. Interface* **2013**, *10*, 20130651. [CrossRef] [PubMed]
52. Manca, F.; Giordano, S.; Palla, P.L.; Cleri, F.; Colombo, L. Two-State Theory of Single-Molecule Stretching Experiments. *Phys. Rev. E Stat. Nonlin. Soft Matter Phys.* **2013**, *87*. [CrossRef]
53. Makarov, D.E. A Theoretical Model for the Mechanical Unfolding of Repeat Proteins. *Biophys. J.* **2009**, *96*, 2160–2167. [CrossRef] [PubMed]
54. Su, T.; Purohit, P.K. Mechanics of Forced Unfolding of Proteins. *Acta Biomater.* **2009**, *5*, 1855–1863. [CrossRef] [PubMed]
55. Dudko, O.K. Decoding the Mechanical Fingerprints of Biomolecules. *Q. Rev. Biophys.* **2016**, *49*, e3. [CrossRef]
56. Rief, M.; Oesterhelt, F.; Heymann, B.; Gaub, H.E. Single Molecule Force Spectroscopy on Polysaccharides by Atomic Force Microscopy. *Science* **1997**, *275*, 129–1297. [CrossRef] [PubMed]
57. Rief, M.; Gautel, M.; Oesterhelt, F.; Fernandez, J.M.; Gaub, H.E. Reversible Unfolding of Individual Titin Immunoglobulin Domains by AFM. *Science* **1997**, *276*, 1109–1112. [CrossRef] [PubMed]
58. Hughes, M.L.; Dougan, L. The Physics of Pulling Polyproteins: A Review of Single Molecule Force Spectroscopy Using the AFM to Study Protein Unfolding. *Rep. Prog. Phys.* **2016**, *79*, 076601. [CrossRef] [PubMed]
59. Benichou, I.; Givli, S. Structures Undergoing Discrete Phase Transformation. *J. Mech. Phys. Solids* **2013**, *61*, 94–113. [CrossRef]
60. Fedelich, B.; Zanzotto, G. Hysteresis in Discrete Systems of Possibly Interacting Elements with a Double-Well Energy. *J. Nonlinear Sci.* **1992**, *2*, 319–342. [CrossRef]

61. Bellino, L.; Florio, G.; Giordano, S.; Puglisi, G. On the Competition between Interface Energy and Temperature in Phase Transition Phenomena. *Appl. Eng. Sci.* **2020**, *2*, 100009. [CrossRef]
62. Cannizzo, A.; Bellino, L.; Florio, G.; Puglisi, G.; Giordano, S. Thermal Control of Nucleation and Propagation Transition Stresses in Discrete Lattices with Non-Local Interactions and Non-Convex Energy. *Eur. Phys. J. Plus* **2022**, *137*. [CrossRef]
63. Huxley, A.F.; Simmons, R.M. Proposed Mechanism of Force Generation in Striated Muscle. *Nature* **1971**, *233*, 533–538. [CrossRef] [PubMed]
64. Hill, T.L. Theory of Muscular Contraction Extended to Groups of Actin Sites. *Proc. Natl. Acad. Sci. USA* **1973**, *70*, 2732–2736. [CrossRef] [PubMed]
65. Caruel, M.; Allain, J.-M.; Truskinovsky, L. Muscle as a Metamaterial Operating near a Critical Point. *Phys. Rev. Lett.* **2013**, *110*, 248103. [CrossRef] [PubMed]
66. Caruel, M.; Truskinovsky, L. Statistical Mechanics of the Huxley-Simmons Model. *Phys. Rev. E* **2016**, *93*, 062407. [CrossRef] [PubMed]
67. Caruel, M.; Truskinovsky, L. Physics of Muscle Contraction. *Rep. Prog. Phys.* **2018**, *81*, 036602. [CrossRef] [PubMed]
68. Giordano, S. Spin Variable Approach for the Statistical Mechanics of Folding and Unfolding Chains. *Soft Matter* **2017**, *13*, 6877–6893. [CrossRef]
69. Benedito, M.; Giordano, S. Thermodynamics of Small Systems with Conformational Transitions: The Case of Two-State Freely Jointed Chains with Extensible Units. *J. Chem. Phys.* **2018**, *149*, 054901. [CrossRef] [PubMed]
70. Benedito, M.; Giordano, S. Isotensional and Isometric Force-Extension Response of Chains with Bistable Units and Ising Interactions. *Phys. Rev. E* **2018**, *98*, 052146. [CrossRef]
71. Benedito, M.; Manca, F.; Giordano, S. Full Statistics of Conjugated Thermodynamic Ensembles in Chains of Bistable Units. *Inventions* **2019**, *4*, 19. [CrossRef]
72. Florio, G.; Puglisi, G. Unveiling the Influence of Device Stiffness in Single Macromolecule Unfolding. *Sci. Rep.* **2019**, *9*, 4997. [CrossRef] [PubMed]
73. Bellino, L.; Florio, G.; Puglisi, G. The Influence of Device Handles in Single-Molecule Experiments. *Soft Matter* **2019**, *15*, 8680–8690. [CrossRef] [PubMed]
74. Benedito, M.; Giordano, S. Unfolding Pathway and Its Identifiability in Heterogeneous Chains of Bistable Units. *Phys. Lett. A* **2020**, *384*, 126124. [CrossRef]
75. Benedito, M.; Manca, F.; Palla, P.L.; Giordano, S. Rate-Dependent Force-Extension Models for Single-Molecule Force Spectroscopy Experiments. *Phys. Biol.* **2020**, *17*, 056002. [CrossRef] [PubMed]
76. Florio, G.; Puglisi, G.; Giordano, S. Role of Temperature in the Decohesion of an Elastic Chain Tethered to a Substrate by Onsite Breakable Links. *Phys. Rev. Res.* **2020**, *2*, 033227. [CrossRef]
77. Cannizzo, A.; Florio, G.; Puglisi, G.; Giordano, S. Temperature Controlled Decohesion Regimes of an Elastic Chain Adhering to a Fixed Substrate by Softening and Breakable Bonds. *J. Phys. A Math. Theor.* **2021**, *54*, 445001. [CrossRef]
78. Winkler, R.G. Equivalence of Statistical Ensembles in Stretching Single Flexible Polymers. *Soft Matter* **2010**, *6*, 6183. [CrossRef]
79. Manca, F.; Giordano, S.; Palla, P.L.; Cleri, F.; Colombo, L. Response to "Comment on Elasticity of Flexible and Semiflexible Polymers with Extensible Bonds in the Gibbs and Helmholtz Ensembles" [J. Chem. Phys. 138, 157101 (2013)]. *J. Chem. Phys.* **2013**, *138*, 157102. [CrossRef] [PubMed]
80. Manca, F.; Giordano, S.; Palla, P.L.; Cleri, F. On the Equivalence of Thermodynamics Ensembles for Flexible Polymer Chains. *Phys. A* **2014**, *395*, 154–170. [CrossRef]
81. Giordano, S. Helmholtz and Gibbs Ensembles, Thermodynamic Limit and Bistability in Polymer Lattice Models. *Contin. Mech. Thermodyn.* **2018**, *30*, 459–483. [CrossRef]
82. Skvortsov, A.M.; Klushin, L.I.; Leermakers, F.A.M. Negative Compressibility and Nonequivalence of Two Statistical Ensembles in the Escape Transition of a Polymer Chain. *J. Chem. Phys.* **2007**, *126*, 024905. [CrossRef]
83. Dimitrov, D.I.; Klushin, L.I.; Skvortsov, A.; Milchev, A.; Binder, K. The Escape Transition of a Polymer: A Unique Case of Non-Equivalence between Statistical Ensembles. *Eur. Phys. J. E Soft Matter* **2009**, *29*, 9–25. [CrossRef] [PubMed]
84. Skvortsov, A.M.; Klushin, L.I.; Polotsky, A.A.; Binder, K. Mechanical Desorption of a Single Chain: Unusual Aspects of Phase Coexistence at a First-Order Transition. *Phys. Rev. E Stat. Nonlin. Soft Matter Phys.* **2012**, *85*, 031803. [CrossRef] [PubMed]
85. Dutta, S.; Benetatos, P. Inequivalence of Fixed-Force and Fixed-Extension Statistical Ensembles for a Flexible Polymer Tethered to a Planar Substrate. *Soft Matter* **2018**, *14*, 6857–6866. [CrossRef]
86. Dutta, S.; Benetatos, P. Statistical Ensemble Inequivalence for Flexible Polymers under Confinement in Various Geometries. *Soft Matter* **2020**, *16*, 2114–2127. [CrossRef] [PubMed]
87. Noh, G.; Benetatos, P. Tensile Elasticity of a Freely Jointed Chain with Reversible Hinges. *Soft Matter* **2021**, *17*, 3333–3345. [CrossRef] [PubMed]
88. Bell, G.I. Models for the Specific Adhesion of Cells to Cells: A Theoretical Framework for Adhesion Mediated by Reversible Bonds between Cell Surface Molecules. *Science* **1978**, *200*, 618–627. [CrossRef] [PubMed]
89. Bell, G.I.; Dembo, M.; Bongrand, P. Cell Adhesion. Competition between Nonspecific Repulsion and Specific Bonding. *Biophys. J.* **1984**, *45*, 1051–1064. [CrossRef]
90. Schlierf, M.; Rief, M. Single-Molecule Unfolding Force Distributions Reveal a Funnel-Shaped Energy Landscape. *Biophys. J.* **2006**, *90*, L33–L35. [CrossRef] [PubMed]

91. Rico, F.; Gonzalez, L.; Casuso, I.; Puig-Vidal, M.; Scheuring, S. High-Speed Force Spectroscopy Unfolds Titin at the Velocity of Molecular Dynamics Simulations. *Science* **2013**, *342*, 741–743. [CrossRef] [PubMed]
92. Manca, F.; Déjardin, P.-M.; Giordano, S. Statistical Mechanics of Holonomic Systems as a Brownian Motion on Smooth Manifolds: Statistical Mechanics of Holonomic Systems as a Brownian Motion. *Ann. Phys.* **2016**, *528*, 381–393. [CrossRef]
93. Giordano, S. Stochastic Thermodynamics of Holonomic Systems. *Eur. Phys. J. B* **2019**, *92*, 174. [CrossRef]
94. Risken, H.; Frank, T.D. *The Fokker-Planck Equation: Methods of Solution and Applications*, 2nd ed.; Springer: Berlin/Heidelberg, Germany, 1989; ISBN 9783540504986.
95. Coffey, W.T.; Kalmykov, Y.P.; Waldron, J.T. *The Langevin Equation: With Applications to Stochastic Problems in Physics, Chemistry and Electrical Engineering*; World Scientific Series in Contemporary Chemical Physics; World Scientific Publishing Company: Singapore, 2004; Volume 14; ISBN 9786611935528.